JMEPEG (2010) 19:1037–1042
DOI: 10.1007/s11665-009-9569-5

1059-9495/$19.00

# Influence of Dispersant and Heat Treatment on the Morphology of Nanocrystalline Hydroxyapatite

*Yusong Pan and Dangsheng Xiong*

*(Submitted December 19, 2008; in revised form September 14, 2009)*

**Natural biological hard tissues are biocomposites of proteins and hydroxyapatite (HA) with superior strength. Nanometer scale HAp is the key material to manufacture bone substitute. In this work, nano-sized HA particles were synthesized by a wet method using orthophosphoric acid and calcium hydroxide as raw materials. The prepared nanocrystalline HAp was characterized for its phase purity and nano-scale morphological structure by XRD, TEM, and FTIR. The influences of heat treatment temperature and dispersant on the properties of HAp were also investigated. The results indicated that nano-particles were pure single-phase HAp with a diameter of 25-70 nm and length of 50-180 nm depending on heat treatment temperature. The morphology and crystallite size of HAp change with heat treatment temperature. After heat treating, the crystallinity of these nano-particles increased and its morphology transformed from needle-like to sphere-like structure. The dispersant is beneficial to prevent the growth of HA particles and provide a uniform particle size distribution. Moreover, the HAp tends to form small agglomerates in the absence of dispersant.**

**Keywords** crystallite size, hydroxyapatite, morphology, wet chemical process

## 1. Introduction

Hydroxyapatite (HAp: $Ca_{10}(PO_4)_6(OH)_2$) is one of the major constituents of the inorganic components in human hard tissues such as bone and teeth. It is used widely for bone implant and bone cement applications due to its compositional and biological similarities to native tissues (Ref 1, 2). Since it is one of the most biocompatible and bioactive materials, it is also a promising material as reinforcing filler for composites, especially used in the medical field. For example, hydrogels, such as poly(vinyl alcohol), collagen, polylactic acid, exhibit excellent biocompatibility and they are widely used as bone tissue scaffold or articular cartilage. However, the hydrogels alone do not have adequate mechanical properties as well as absence of bioactivity for various biomedical applications including scaffold tasks. Compounding of hydrogels and hydroxyapatite can provide not only improved mechanical properties, but also excellent bioactivity (Ref 3-6). Moreover, HA is also used as a coating biomaterial due to its perfect bioactive properties. The development of coatings with hydroxyapatite for orthopedic and dental applications offers a large number of advantages, such as surface metallic covering, bond to surrounding osseous tissue, and bone formation enhancement (Ref 7-9).

**Yusong Pan**, Department of Material Science and Engineering, Anhui University of Science and Technology, Huainan 232001, China; and **Dangsheng Xiong**, Department of Material Science and Engineering, Nanjing University of Science and Technology, Nanjing 210094, China. Contact e-mail: yusongpan@163.com.

In recent years, synthetic hydroxyapatite has been widely used in various clinical applications due to its compositional similarity to the mineral phase present in hard tissue of human body. Many methods such as hydrolysis, sol-gel, hydrothermal, and solid-state reaction methods have been employed to synthesize HAp crystals with different morphologies (Ref 10-13). The most commonly used technique for the formation of HAp crystals is the precipitation technique, involving wet chemical reactions between the calcium and phosphate precursors under controlled temperature and pH conditions (Ref 14, 15). Akao et al. (Ref 16) previously prepared HA powders based on the use of the following reaction of calcium hydroxide with orthophosphoric acid:

$$10Ca(OH)_2 + 6H_3PO_4 \rightarrow Ca_{10}(PO_4)_6(OH)_2 + 18H_2O \quad \text{(Eq 1)}$$

This method is suitable for a biomedical production of HA since the only by-product is water and no toxic product is introduced.

In this paper, nano-sized HAp has been successfully prepared by direct precipitation reaction of $Ca(OH)_2$ and $H_3PO_4$ solutions. All the reaction processes were carried out in the solution at 80 °C in water bath. The present method is simple and needs neither extreme conditions such as high temperature, pressure, and protective gas nor complex apparatus. Here we focused on the study of influences of dispersant as well as heat treatment temperature on the morphology and size of HA.

## 2. Materials and Methods

### 2.1 Starting Materials

Calcium hydroxide and orthophosphoric acid were used as starting materials to prepare HA powders. Ammonium hydroxide solution was used to adjust pH value and poly vinyl alcohol

(PVA 500) was used as dispersant. All the chemical reagents used here were analytical grade and acquired from Siopharm chemical reagent Co., Ltd., Shanghai, China.

### 2.2 Preparation of Hydroxyapatite

HA powders were prepared by a wet chemical synthesis technique, based on the precipitation of HA particles from aqueous solutions. The synthesis procedure involved the drop by drop introduction of the $H_3PO_4$ solution (100 mL, 0.6 M) into an aqueous suspension of $Ca(OH)_2$ (125 mL, 0.8 M) while stirring vigorously for about 2 h at 80 °C. Simultaneously, ammonia hydroxide solution was added to adjust pH at 10-11. Then, the obtained white precipitate was aged for 24 h at 70 °C, decanted, rinsed with deionized water until its pH reached to about 7. After filtration, the precipitate was dried in vacuum oven at 70 °C for 24 h. Finally, in order to study the effects of heat treatment on the synthesized HA powders, they were heated at 500 and 900 °C for 1 h in a conventional furnace under air atmosphere, respectively.

In order to investigate the influences of dispersant on the morphology of HA, HA powders were prepared with or without the presence of dispersant, respectively.

### 2.3 X-Ray Diffraction Analysis

Chemical composition, structure, and crystallinity of nanocrystalline HAp were determined by x-ray powder diffraction (XRD). XRD experiments were performed on HA powder with a diffractometer (2038, REGAKU, Japan), using Cu Kα radiation (λ = 1.5406 A) at 33 kV and current 15 mA. Samples were scanned over 2θ range of 15-70° and the step size of scanning is 0.02°.

### 2.4 FTIR Spectroscopy

Fourier transform infrared (FTIR) spectroscopy (MB154S, BOMEM, Canada) was used to identify the functional groups of HA powder. A dried sample of 2 mg was carefully mixed with 200 mg of KBr and pressed into a pellet under a hydraulic pressure. The spectrum was recorded in the 4000-500 $cm^{-1}$ region with 2 $cm^{-1}$ resolution. Spectrum analyses were performed using standard Microcal Origin software.

### 2.5 TEM Microscopy

Morphological characterization of the nanometer HAp samples was carried out using transmission electron microscopy (TEM) (JEM 2100, JEOL, Japan). The samples for TEM observation were prepared by dispersing HA powders in anhydrous ethanol and immersing them in an ultrasonic bath for 30 min, and a few drops of the resulting suspension were placed onto a copper grid coated with a layer of amorphous carbon on filter paper and drying in air.

## 3. Results and Discussion

### 3.1 XRD Analysis

Figure 1 shows the XRD patterns of the HA powder vacuum dried at 70 °C and those after heat treatment at 500 and 900 °C, respectively. The XRD phase analysis has been performed using JCPDS card number 09-0432. It can be concluded from Fig. 1 that the XRD peaks of all three diffraction patterns agree well

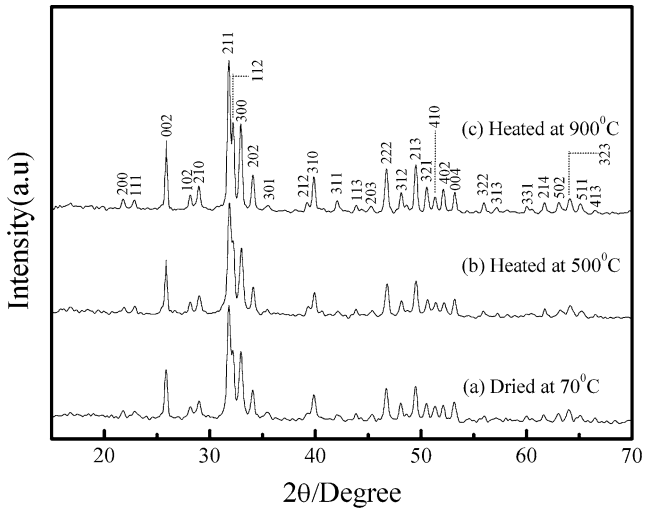


**Fig. 1** XRD patterns of HAp at various heat treatment temperatures (a) 70 °C for 24 h; (b) 500 °C for 1 h; (c) 900 °C for 1 h

with those of standard HA in the powder diffraction file (Card No. 09-432). This result shows that the single-phase hydroxyapatite was prepared and second phase was not detected. The wide and high peaks reveal that the HA powder has a very small size and excellent crystal quality. Moreover, the difference of the intensity and width of the peaks among the three diffraction patterns shown in Fig. 1 was observed. It shows that the intensity of the peaks increases with an increase of the heat treatment temperature. Contrarily, the width of the peaks presents decreasing trend as the heat treatment temperature increases. This suggests that the heat treatment temperature has perceivable effect on the characteristics of HAp. Both the crystallinity and crystallite size of HA increase with the rise of heat treatment temperature. The crystallite size of the HA particles can be determined by Scherrer equation (Ref 17).

$$D = \frac{K\lambda}{\beta \cos \theta} \qquad \text{(Eq 2)}$$

where $D$ is the average crystallite size, β the corrected full width of the peak at half of the maximum intensity, λ the wavelength of x-ray radiation, and $K$ is a constant related to the crystallite shape and is approximately equal to unity.

It can be deduced from Eq 2 that the width of peak is inversely proportional to the average crystallite size, $D$. Figure 2 shows the effect of heat treatment temperature on the crystallite size of HAp, which is calculated using the diffraction peaks of (002) plane according to Scherrer equation. The calculation result indicates that the crystallite size of HAp increases with an increase in the temperature, especially in the high temperature region. For example, the crystallite size of HAp increases from 25.2 to 37.5 nm, only increasing 49%, while the temperature rising from 70 to 500 °C. It almost increases 72% as the temperature increasing from 500 to 900 °C.

To investigate the effect of dispersant on the quality of crystallization and particle size of HAp, hydroxyapatite particles were prepared in the presence and in the absence of dispersant, respectively. The results of XRD pattern are shown in Fig. 3. The wide and high peaks reveal that the HAp has a small size and excellent crystal quality and the diffraction data are consistent with JCPDS file no. 09-432. No impurity other

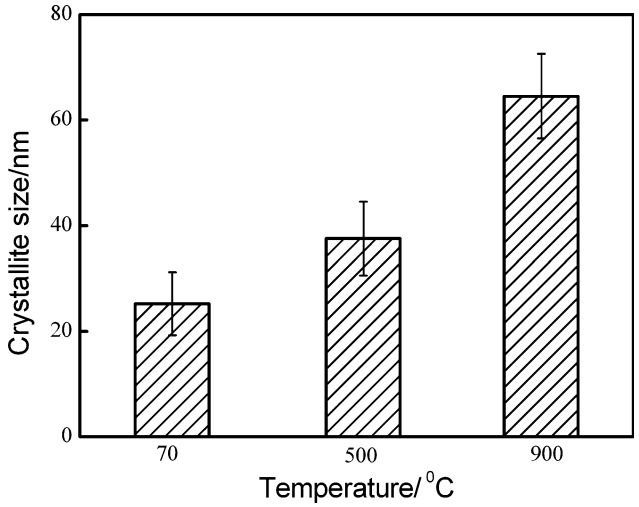


**Fig. 2** The effect of heat treatment temperature on the crystallite size of HA

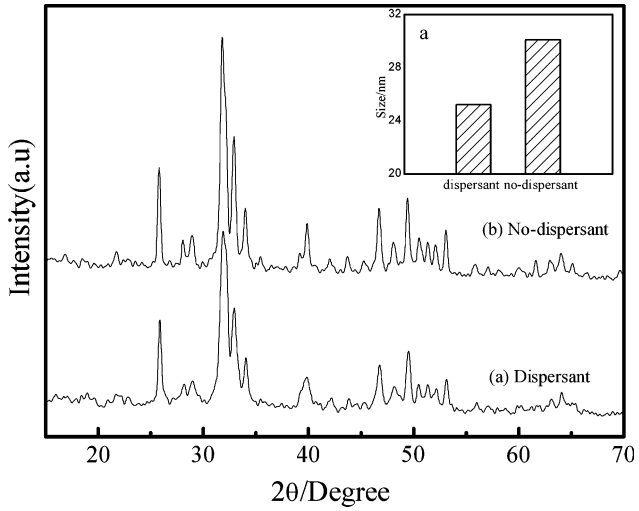


**Fig. 3** The effect of dispersant on the formation of HAp (a) with dispersant, (b) without dispersant

than HAp is detected by XRD. The intensity of HA prepared in the presence of dispersant is weaker than that of HA prepared in the absence of dispersant, but the full width of the peak at half of the maximum intensity of HA broadened in the presence of dispersant. The results indicate that the dispersant of PVA is beneficial to prevent the growth of HA particle, but the crystallinity of HA in the presence of dispersant also lowers. The crystallite size of HAp that was calculated using the diffraction peaks of (002) plane according to Scherrer equation is presented in the inset (a) of Fig. 3. The calculation result indicates that the crystallite size of HAp increases from 25.2 nm in the presence of the dispersant to 30.1 nm in the absence of dispersant.

### 3.2 FTIR Studies

Figure 4(a-c) illustrates FTIR spectra of hydroxyapatite heated at various temperatures, i.e., 70, 500, and 900 °C, respectively. The infrared band positions and their assignments

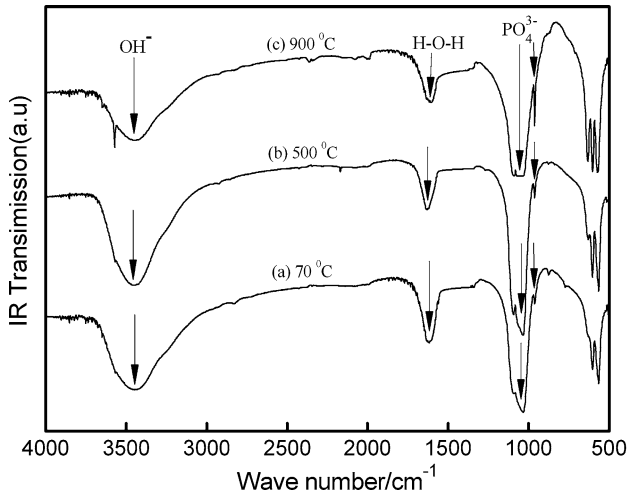


**Fig. 4** FTIR spectra of HA. (a) Dried HA at 70 °C; (b) heated HA at 500 °C; (c) heated HA at 900 °C

**Table 1 Assignments of the observed vibrational frequencies of HA particle heated at different temperatures**

| | Observed vibrational frequencies, $cm^{-1}$ | | |
|---|---|---|---|
| **Assignments** | **70 °C** | **500 °C** | **900 °C** |
| Structural $OH^-$ | ... | ... | 3572 |
| $H_2O$ absorbed | 3448 | 3448 | 3448 |
| $H_2O$ absorbed ($\nu_2$) | 1629 | 1628 | 1628 |
| $PO_4^{3-}$ bend $\nu_3$ | 1033 | 1033 | 1045 |
| $PO_4^{3-}$ stretch $\nu_1$ | 962 | 962 | 962 |
| Structural $OH^-$ | 632 | 632 | 630 |
| $PO_4^{3-}$ bend $\nu_4$ | 603 | 603 | 602 |
| $PO_4^{3-}$ bend $\nu_4$ | 565 | 565 | 572 |

are summarized in Table 1. Absorption peaks at 882, 1421, and 1460 $cm^{-1}$ for carbonate ions have not been observed in the as-made materials (Ref 18). This observation indicates that the prepared materials are only composed of HAp. In the IR spectra, the fact that all the spectra possess broad bands at 3500-3400 $cm^{-1}$ and 1629 $cm^{-1}$ is an indication of strongly adsorbed and/or bound water in the materials (Ref 18, 19). A sharp and strong band appears at 3572 $cm^{-1}$ due to the vibration of hydroxyl ions as the heat processing temperature increased. The strongest peak at 1033 $cm^{-1}$ and bands at 565 and 603 $cm^{-1}$ are attributed to the bending vibration of $PO_4^{3-}$ (Ref 20).

The band (bending) due to structural OH in HA also occurs at around 630 $cm^{-1}$. These peaks for materials heated at 70 and 500 °C appear as weak shoulders that gradually deepen and they merge to become a well-developed peak after heating at 900 °C. For clarity, these features are shown in Fig. 5. This evolution also indicates good crystallinity for the materials heated at higher temperatures. It is believed that IR band at 631 $cm^{-1}$ is absent in carbonate apatite (Ref 21). This result also suggests that no carbonate substitution in HA particles occurred after it being exposed to elevated heat treatment temperature.

### 3.3 TEM Investigation

The TEM micrographs of HA particles prepared with and without dispersant are shown in Fig. 6. These micrographs clearly indicate that the size of precipitated HA particles prepared by wet chemical method is on the nanometer scale. The comparison of the relative micrographs of Fig. 6(a) and (b) reveals some significant changes between morphology and size of the particles. The morphology of HAp shown in Fig. 6(a) presents needle-like crystals with an average size of approximately 25-30 nm in width and 180-200 nm in length. In Fig. 6(b), HA particles hold rod-like crystals and congregation also can be observed. The results indicate that the dispersant has an obvious influence on the morphology and size of HA particles. It can be concluded that the dispersant may prevent the growth of HA particles and provide a more uniform size distribution. The results of the TEM analysis agree well with the analysis of XRD pattern.

Liu et al. (Ref 20) has investigated the effect of PEG and cetylrimethyl ammonium bromide (CTAB) as dispersant on the morphology of HA particles. The resultant also shows needle-like structure of HA particle in the presence of CTAB and PEG. The effect of CTAB and PEG on the formation of HAp is attributed to the following: (1) PEG is a nonionic surfactant. The PEG monomer can easily form long chain structures in aqueous solution. (2) In an aqueous system, CTAB would ionize completely and result in a cation with tetrahedral structure. (3) The phosphate anion is also a tetrahedral structure. In this study, PVA is also a nonionic surfactant whose structure is similar to that of PEG. From Fig. 6, it is proposed that the PVA possesses the ability to control the crystal growth process as well as to prevent conglomeration of HA particles. Therefore, HAp nano-particles may grow along the long chains of PVA and needle-like structures formed when $Ca^{2+}$ ions meet $PO_4^{3-}$ and $OH^-$ ions. Hence, PVA may be used as a soft template in the synthesis of HA particles.

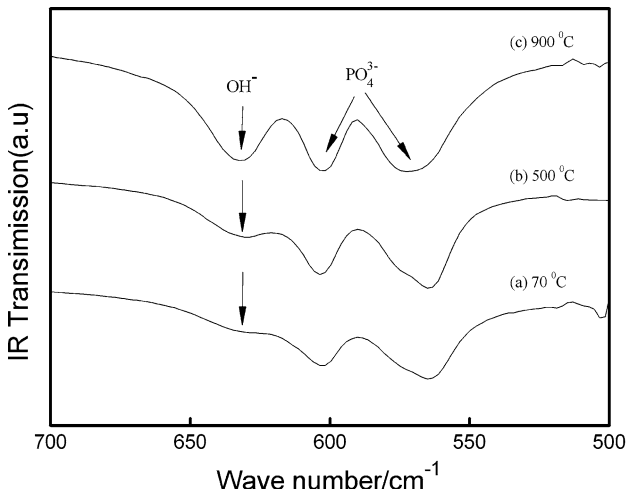


**Fig. 5** FTIR spectra of narrow scan for HA particles heated at different temperatures: (a) 70 °C, (b) 500 °C, and (c) 900 °C

Figure 7 shows the microstructure of HA particles after heat treatment at different temperatures. It can be clearly seen that the particles have grown and their morphology has changed from needle-like to spherical while the heat treatment temperature rises from 70 to 900 °C. The results indicate that the heat treatment has a drastic effect on the morphology of HAp crystals synthesized by wet chemical methods. The HAp crystals experience a process of morphological and size transition when the heat treatment temperature increases gradually. In Fig. 7(a), large numbers of nano-sized needle-like crystals are distributed randomly. With the increase of heat treatment temperature to 500 °C, most HAp crystals congregated and their morphology changed from needle-like to short rod-like (Fig. 7b). While the heat treatment temperature increased further, these short rod-like crystals transformed into large spherical HA particles with an average size about 65-75 nm in diameter, as shown in Fig. 7(c).

In order to quantitatively estimate the effect of heat treatment temperature on the morphology of HA particles, it can be evaluated by shape factor ($F_r$), which is defined as follows:

$$F_r = \frac{L}{D} \quad \text{(Eq 3)}$$

where $L$ is the average length and $D$ is the average width of HA crystallite, respectively. In this paper, $L$ and $D$ are measured according to TEM micrograph. The calculated

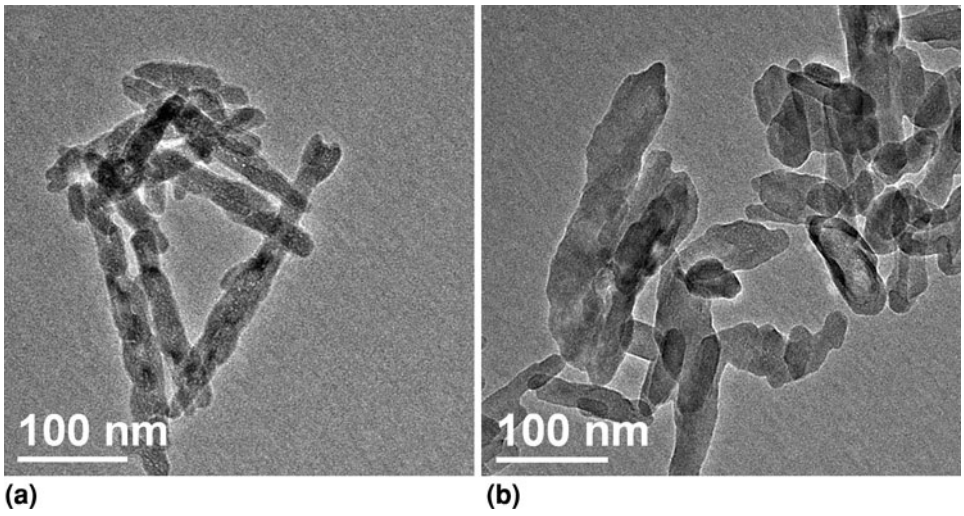


**Fig. 6** TEM micrograph of HA particles dried at 70 °C (a) with dispersant, (b) without dispersant

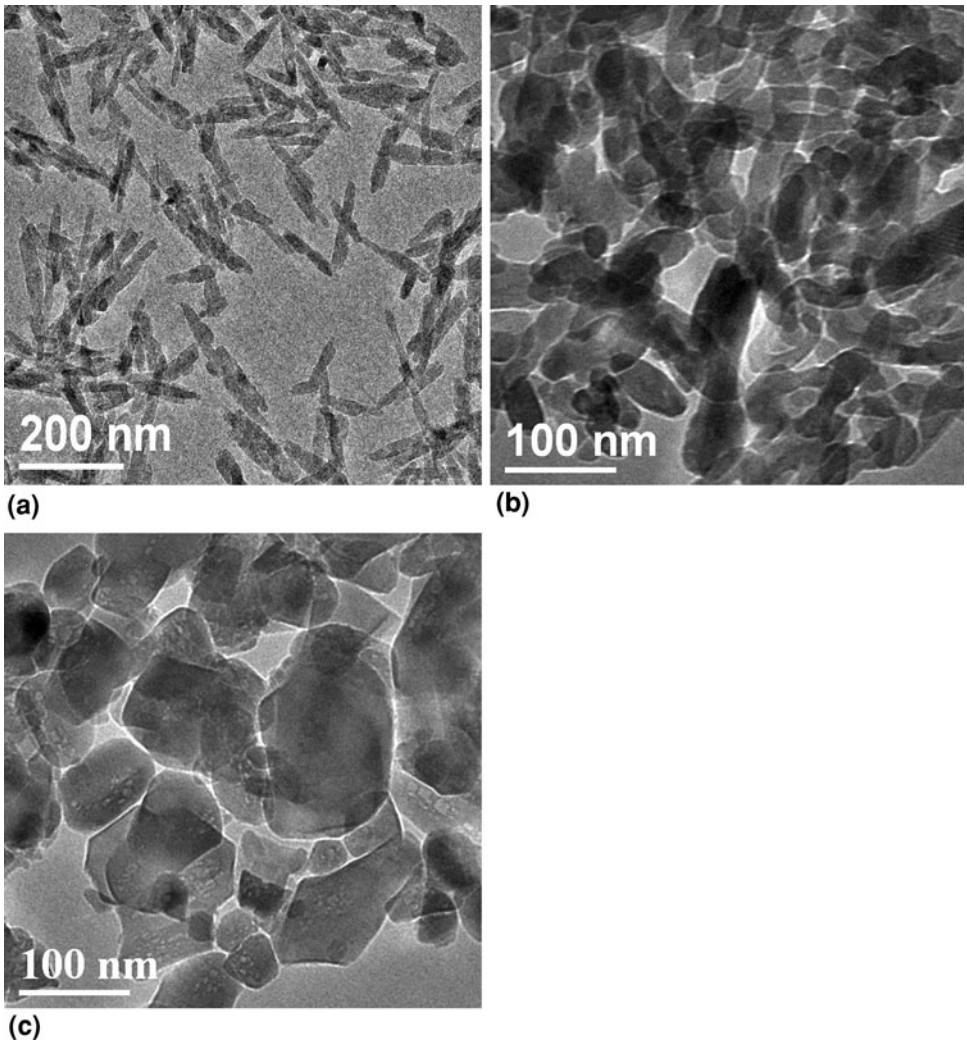


**Fig. 7** TEM micrograph of HA particles prepared with dispersant (a) dried at 70 °C, (b) heated at 500 °C, and (c) heated at 900 °C

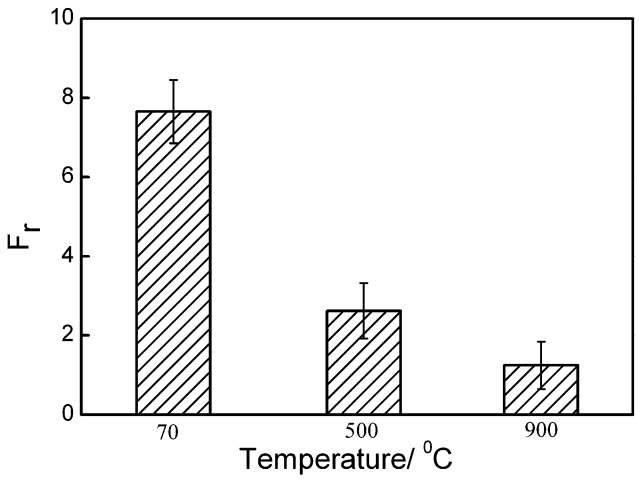


**Fig. 8** The effect of temperature on the morphology of HA particle

results of $F_r$ at different heat treatment temperatures are shown in Fig. 8. It can be concluded that the value of shape factor decreased greatly with the increase of heating temperature. For example, the value of shape factor decreases from 7.65 at 70 °C to 1.25 at 900 °C. These values of $F_r$ also suggest that the morphology of HA particles transforms from needle-like to sphere-like and this behavior is consistent with the observed microstructure of HA particles by TEM.

## 4. Conclusions

In this study, nano-scale HA particles were successfully prepared by wet chemical technique. XRD and FTIR studies confirmed the high purity and crystallinity of HAp crystals obtained. The product is very pure, without carbonated HAps. The morphology and size of the HAp significantly depend on the heat treatment temperature and dispersant. Both the crystallinity and the crystallite size of HAp increased with the rise of heat treatment temperature. The morphology of HAp transformed from needle-like to sphere-like shape while the heat treatment temperature increased from 70 to 900 °C. In addition, PVA as a dispersant is beneficial to prevent the growth of HA particle and the crystallinity of HAp in the presence of dispersant is lowered.

## Acknowledgments

This research was supported by the National Natural Science Foundation of China and by the national high technology research and development program of China.

## References

1. T.D. Roy, J.R. Simon, J.L. Ricci, E.D. Rekow, V.P. Thompson, and J.R. Parsons, Performance of Hydroxyapatite Bone Repair Scaffolds Created via Three-Dimensional Fabrication Techniques, *J. Biomed. Mater. Res. A*, 2003, **67**(4), p 1228–1237
2. J. Brandt, S. Henning, G. Michler, M. Schulz, and A. Bernstein, Nanocrystalline Hydroxyapatite for Bone Repair, *Key Eng. Mater.*, 2008, **361-363**, p 35–38
3. Y.S. Pan and D.S. Xiong, Friction Properties of Nano-hydroxyapatite Reinforced Poly(Vinyl Alcohol) Gel Composites as an Articular Cartilage, *Wear*, 2009, **266**(7–8), p 699–703
4. J. Ren, P. Zhao, T. Ren, S.Y. Gu, and K.F. Pan, Poly (D,L-Lactide)/Nano-Hydroxyapatite Composite Scaffolds for Bone Tissue Engineering and Biocompatibility Evaluation, *J. Mater. Sci. Mater. Med.*, 2008, **19**(3), p 1075–1082
5. N. Fukui, T. Sato, Y. Kuboki, and A. Aoki, Bone Tissue Reaction of Nano-Hydroxyapatite/Collagen Composite at the Early Stage of Implantation, *Bio-Med. Mater. Eng.*, 2008, **18**(1), p 25–33
6. J. Song, J.W. Xu, T. Filion, E. Saiz, A.P. Tomsia, and J.B. Lian, Elastomeric High-Mineral Content Hydrogel-Hydroxyapatite Composites for Orthopedic Applications, *J. Biomed. Mater. Res. A*, 2009, **89**(4), p 1098–1107
7. C.T. Kwok, P.K. Wong, F.T. Cheng, and H.C. Man, Characterization and Corrosion Behavior of Hydroxyapatite Coatings on Ti6Al4V Fabricated by Electrophoretic Deposition, *Appl. Surf. Sci.*, 2009, **255**(13–14), p 6736–6744
8. X.F. Xiao, R.F. Liu, and Y.Z. Zheng, Characterization of Hydroxyapatite/Titania Composite Coatings Codeposited by a Hydrothermal-Electrochemical Method on Titanium, *Surf. Coat. Technol.*, 2006, **200**(14–15), p 4406–4413
9. J. Chakraborty, M.K. Sinha, and D. Basu, Biomolecular Template-Induced Biomimetic Coating of Hydroxyapatite on an SS 316 L Substrate, *J. Am. Ceram. Soc.*, 2007, **90**(4), p 1258–1261
10. W.J. Shih, J.W. Wang, M.C. Wang, and M.H. Hon, A Study on the Phase Transformation of the Nanosized Hydroxyapatite Synthesized by Hydrolysis Using In Situ High Temperature X-Ray Diffraction, *Mater. Sci. Eng.*, 2006, **26**(8), p 1434–1438
11. U. Vijayalakshmi, K. Prabakaran, and S. Rajeswari, Preparation and Characterization of Sol-Gel Hydroxyapatite and Its Electrochemical Evaluation for Biomedical Applications, *J. Biomed. Mater. Res. B*, 2008, **87**(3), p 739–749
12. X.F. Xiao, R.F. Liu, and Y.J. Gao, Hydrothermal Preparation of Nanocarbonated Hydroxyapatite Crystallites, *Mater. Sci. Technol.*, 2008, **24**(10), p 1199–1203
13. J.M. Cao, J. Feng, S.G. Deng, X. Chang, J. Wang, J.S. Liu, and S. Jin, Microwave-Assisted Solid-State Synthesis of Hydroxyapatite Nanorods at Room Temperature, *J. Mater. Sci.*, 2005, **40**(23), p 6311–6313
14. M.R. Saeri, A. Afshar, M. Ghorbani, N. Ehsani, and C.C. Sorrell, The Wet Precipitation Process of Hydroxyapatite, *Mater. Lett.*, 2003, **57**, p 4064–4069
15. S. Madhavi, C. Ferraris, and T.J. White, Synthesis, Crystallization of Macroporous Hydroxyapatite, *J. Solid State Chem.*, 2005, **178**, p 2838–2845
16. M. Akao, H. Aoki, and K. Kato, Mechanical Properties of Sintered Hydroxyapatite for Prosthetic Applications, *Mater. Sci.*, 1981, **16**(3), p 809–812
17. V.M. Rusu, C.H. Ng, M. Wilke, B. Tiersch, P. Fratzl, and M.G. Peter, Size-Controlled Hydroxyapatite Nanoparticles as Self-Organized Organic-Inorganic Composite Materials, *Biomaterials*, 2005, **26**, p 5414–5426
18. R.N. Panda, M.F. Hsieh, R.J. Chung, and T.S. Chin, FTIR, XRD, SEM and Solid State NMR Investigations of Carbonate-Containing Hydroxyapatite Nano-Particles Synthesized by Hydroxide-Gel Technique, *J. Phys. Chem. Solids*, 2003, **64**, p 193–199
19. F. Chen, Z.C. Wang, and C.J. Lin, Preparation and Characterization of Nano-Sized Hydroxyapatite Particles and Hydroxyapatite/Chitosan Nano-Composite for use in Biomedical Materials, *Mater. Lett.*, 2002, **57**, p 858–861
20. Y.K. Liu, D.D. Houm, and G.H. Wang, A Simple Wet Chemical Synthesis and Characterization of Hydroxyapatite Nanorods, *Mater. Chem. Phys.*, 2004, **86**, p 69–73
21. N. Sahai and J.A. Tossell, Molecular Orbital Study of Apatite ($Ca_5(PO_4)_3OH$) Nucleation at Silica Bioceramic Surfaces, *J. Phys. Chem. B*, 2000, **104**(18), p 4322–4341